Model-independent analysis of four-fermion contact interaction at e^+e^- collider

A.A. Pankov

Technical University of Gomel, 246746 Belarus

Abstract

We study electron-electron contact-interaction searches in the processe $e^+e^- \to e^+e^-$ at a future e^+e^- Linear Collider with both beams longitudinally polarized. We evaluate the model-independent constraints on the coupling constants, emphasizing the role of beam polarization, and make a comparison with the case of $e^+e^- \to \mu^+\mu^-$.

1 Introduction

Deviations from the Standard Model (SM) caused by new physics characterized by very high mass scales Λ can systematically be studied at lower energies by using the effective Lagrangian approach. In this framework, by integration of the heavy degrees of freedom of the new theory, an effective Lagrangian which obeys the low energy SM symmetries is constructed in terms of the SM fields. The resulting interaction consists of the SM itself as the leading term, plus a series of higher order terms represented by higher-dimensional local operators that are suppressed by powers of the scale Λ. Consequently, the effects of the new physics can be observed at energies well-below Λ as a deviations from the SM predictions, and can be related to some effective contact interaction.

We consider the effects of the flavor-diagonal, helicity conserving, $eeff$ contact-interaction effective Lagrangian [1]

$$\mathcal{L}_{\rm CI} = \frac{1}{1+\delta_{ef}} \sum_{i,j} g_{\rm eff}^2 \, \epsilon_{ij} \left(\bar{e}_i \gamma_\mu e_i\right) \left(\bar{f}_j \gamma^\mu f_j\right), \tag{1}$$

in the Bhabha scattering process

$$e^+ + e^- \to e^+ + e^-, \tag{2}$$

at an e^+e^- Linear Collider (LC) with c.m. energy $\sqrt{s} = 0.5\,\text{TeV}$ and polarized electron and positron beams [2]. In Eq. (1): $i, j = \text{L}, \text{R}$ denote left- or right-handed fermion helicities, f indicates the fermion species, so that $\delta_{ef} = 1$ for the process (2) under consideration, and the CI coupling constants are parameterized in terms of corresponding mass scales as $\epsilon_{ij} = \eta_{ij}/\Lambda_{ij}^2$. Actually, one assumes $g_{\rm eff}^2 = 4\pi$ to account for the fact that the interaction would become strong at $\sqrt{s} \simeq \Lambda$, and by convention $|\eta_{ij}| = \pm 1$ or $\eta_{ij} = 0$, leaving the energy scales Λ_{ij} as free, *a priori* independent parameters.

Clearly, at $s \ll \Lambda_{ij}^2$, the Lagrangian (1) can only contribute virtual effects, to be sought for as very small deviations of the measured observables from the Standard Model (SM) predictions. The relative size of such effects are expected to be of order $s/\alpha\Lambda^2$, with α the SM coupling (essentially, the fine structure constant) and, therefore, very high collider energies and luminosities are required for this kind of searches. In practice, the constraints and the attainable reach on the CI couplings can be numerically assessed by comparing the theoretical deviations with the foreseen experimental uncertainties on the cross sections.

For the case of the Bhabha process (2), the effective Lagrangian interaction in Eq. (1) envisages the existence of six individual, and independent, CI models, contributing to individual helicity amplitudes or combinations of them, with *a priori* free, and nonvanishing, coefficients (basically, $\epsilon_{\rm LL}, \epsilon_{\rm RR}$ and $\epsilon_{\rm LR}$ combined with the $\pm$ signs). Correspondingly, in principle the most general, and model-independent, analysis of the data must account for the situation where all four-fermion effective couplings defined in Eq. (1) are simultaneously allowed in the expression for the cross section. Potentially, the different CI couplings may interfere and substantially weaken the bounds. Indeed, although the different helicity amplitudes by themselves do not interfere, *the deviations from the SM* could be positive

for one helicity amplitude and negative for another, so that accidental cancellation might occur in the sought for deviations from the SM predictions for the relevant observables.

The simplest attitude is to assume non-zero values for only one of the couplings (or one specific combination of them) at a time, with all others zero, this leads to tests of the specific models mentioned above. Also, in many cases, global analyses combining data from different experiments relevant to the considered type of coupling are performed. Current lower bounds on the corresponding Λ's obtained along this line from recent analyses of $e^+e^- \to \bar{f}f$ at LEP, that include Bhabha scattering, are in the range 8-20 TeV and are found to substantially depend on the considered one-parameter scenario [3, 4]. Examples of results for the $eeff$ couplings for the different fermion species in (1), from analyses of different kinds of processes and experiments, can be found, *e.g.*, in Refs. [5–9].

It should be highly desirable to apply a more general (and model-independent) approach to the analysis of experimental data, that allows to simultaneously include all terms of Eq. (1) as independent, non vanishing free parameters, and yet to derive separate constraints (or exclusion regions) on the values of the CI coupling constants, free from potential weakening due to accidental cancellations.

Such an analysis is feasible with initial beam longitudinal polarization, a possibility envisaged at the LC, that allows to extract the individual helicity cross sections from suitable combinations of measurable polarized cross sections and, consequently, to disentangle the constraints on the corresponding CI constants ϵ_{ij}, see,*e.g.*, Refs. [10–17]. In what follows, we wish to complement the model-independent analysis of $e^+e^- \to \bar{f}f$ with $f \neq e, t$ given in Refs. [16, 17], with a discussion of the role of the polarized differential cross sections measurable at the LC in the derivation of model-independent bounds on the three independent four-electron contact interactions relevant to the Bhabha process (2).

2 Observables

With P^- and P^+ the longitudinal polarization of the electron and positron beams, respectively, and θ the angle between the incoming and the outgoing electrons in the c.m. frame, the differential cross section of process (2) at lowest order, including γ and Z exchanges both in the s and t channels and the contact interaction (1), can be written in the following form [10, 11, 14]:

$$\frac{\mathrm{d}\sigma(P^-,P^+)}{\mathrm{d}\cos\theta} = (1-P^-P^+)\,\frac{\mathrm{d}\sigma_1}{\mathrm{d}\cos\theta} + (1+P^-P^+)\,\frac{\mathrm{d}\sigma_2}{\mathrm{d}\cos\theta} + (P^+-P^-)\,\frac{\mathrm{d}\sigma_P}{\mathrm{d}\cos\theta}. \qquad (3)$$

In Eq. (3):

$$\begin{aligned}
\frac{\mathrm{d}\sigma_1}{\mathrm{d}\cos\theta} &= \frac{\pi\alpha^2}{4s}\left[A_+(1+\cos\theta)^2 + A_-(1-\cos\theta)^2\right], \\
\frac{\mathrm{d}\sigma_2}{\mathrm{d}\cos\theta} &= \frac{\pi\alpha^2}{4s}\,4A_0, \\
\frac{\mathrm{d}\sigma_P}{\mathrm{d}\cos\theta} &= \frac{\pi\alpha^2}{4s}\,A_+^P(1+\cos\theta)^2, \qquad (4)
\end{aligned}$$

with

$$
\begin{aligned}
A_0(s,t) &= \left(\frac{s}{t}\right)^2 \left|1 + g_{\rm R}\, g_{\rm L} \chi_Z(t) + \frac{t}{\alpha}\,\epsilon_{\rm LR}\right|^2, \\
A_+(s,t) &= \frac{1}{2}\left|1 + \frac{s}{t} + g_{\rm L}^2\,\left(\chi_Z(s) + \frac{s}{t}\,\chi_Z(t)\right) + 2\frac{s}{\alpha}\,\epsilon_{\rm LL}\right|^2 \\
&+ \frac{1}{2}\left|1 + \frac{s}{t} + g_{\rm R}^2\,\left(\chi_Z(s) + \frac{s}{t}\,\chi_Z(t)\right) + 2\frac{s}{\alpha}\,\epsilon_{\rm RR}\right|^2, \\
A_-(s,t) &= \left|1 + g_{\rm R}\, g_{\rm L}\, \chi_Z(s) + \frac{s}{\alpha}\,\epsilon_{\rm LR}\right|^2, \\
A_+^P(s,t) &= \frac{1}{2}\left|1 + \frac{s}{t} + g_{\rm L}^2\,\left(\chi_Z(s) + \frac{s}{t}\,\chi_Z(t)\right) + 2\frac{s}{\alpha}\,\epsilon_{\rm LL}\right|^2 \\
&- \frac{1}{2}\left|1 + \frac{s}{t} + g_{\rm R}^2\,\left(\chi_Z(s) + \frac{s}{t}\,\chi_Z(t)\right) + 2\frac{s}{\alpha}\,\epsilon_{\rm RR}\right|^2. \qquad (5)
\end{aligned}
$$

Here: α is the fine structure constant; $t = -s(1-\cos\theta)/2$ and $\chi_Z(s) = s/(s - M_Z^2 + iM_Z\Gamma_Z)$, $\chi_Z(t) = t/(t - M_Z^2)$ represent the Z propagator in the s and t channels, respectively, with M_Z and Γ_Z the mass and width of the Z; $g_{\rm R} = \tan\theta_W$, $g_{\rm L} = -\cot 2\,\theta_W$ are the SM right- and left-handed electron couplings of the Z, with θ_W the electroweak mixing angle.

With both beams polarized, the polarization of each beam can be changed on a pulse by pulse basis. This would allow the separate measurement of the polarized cross sections for each of the four polarization configurations $++$, $--$, $+-$ and $-+$, corresponding to the four sets of beam polarizations $(P^-, P^+) = (P_1, P_2)$, $(-P_1, -P_2)$, $(P_1, -P_2)$ and $(-P_1, P_2)$, respectively, with $P_{1,2} > 0$. Specifically, with the simplifying notation $\mathrm{d}\sigma \equiv \mathrm{d}\sigma/\mathrm{d}\cos\theta$:

$$
\begin{aligned}
\mathrm{d}\sigma_{++} &\equiv \mathrm{d}\sigma(P_1, P_2) = (1 - P_1P_2)\,\mathrm{d}\sigma_1 + (1 + P_1P_2)\,\mathrm{d}\sigma_2 + (P_2 - P_1)\,\mathrm{d}\sigma_P, \\
\mathrm{d}\sigma_{--} &\equiv \mathrm{d}\sigma(-P_1, -P_2) = (1 - P_1P_2)\,\mathrm{d}\sigma_1 + (1 + P_1P_2)\,\mathrm{d}\sigma_2 - (P_2 - P_1)\,\mathrm{d}\sigma_P, \\
\mathrm{d}\sigma_{+-} &\equiv \mathrm{d}\sigma(P_1, -P_2) = (1 + P_1P_2)\,\mathrm{d}\sigma_1 + (1 - P_1P_2)\,\mathrm{d}\sigma_2 - (P_2 + P_1)\,\mathrm{d}\sigma_P, \\
\mathrm{d}\sigma_{-+} &\equiv \mathrm{d}\sigma(-P_1, P_2) = (1 + P_1P_2)\,\mathrm{d}\sigma_1 + (1 - P_1P_2)\,\mathrm{d}\sigma_2 + (P_2 + P_1)\,\mathrm{d}\sigma_P. \qquad (6)
\end{aligned}
$$

To extract from the measured polarized cross sections the values of $\mathrm{d}\sigma_1$, $\mathrm{d}\sigma_2$ and $\mathrm{d}\sigma_P$, that carry the information on the CI couplings, one has to invert the system of equations (6). The solution reads:

$$
\begin{aligned}
\mathrm{d}\sigma_1 &= \frac{1}{8}\left[(1 - \frac{1}{P_1P_2})\,(\mathrm{d}\sigma_{++} + \mathrm{d}\sigma_{--}) + (1 + \frac{1}{P_1P_2})\,(\mathrm{d}\sigma_{+-} + \mathrm{d}\sigma_{-+})\right], \\
\mathrm{d}\sigma_2 &= \frac{1}{8}\left[(1 + \frac{1}{P_1P_2})\,(\mathrm{d}\sigma_{++} + \mathrm{d}\sigma_{--}) + (1 - \frac{1}{P_1P_2})\,(\mathrm{d}\sigma_{+-} + \mathrm{d}\sigma_{-+})\right], \\
\mathrm{d}\sigma_P &= -\frac{1}{2\,(P_1 + P_2)}\,(\mathrm{d}\sigma_{+-} - \mathrm{d}\sigma_{-+}) = \frac{1}{2\,(P_2 - P_1)}\,(\mathrm{d}\sigma_{++} - \mathrm{d}\sigma_{--})\,. \qquad (7)
\end{aligned}
$$

Notice that the equations in (6) are not all linearly independent, and that not only $P_1 \neq 0$ and $P_2 \neq 0$, but also $P_1 \neq P_2$ is needed to obtain Eqs. (7). As one can see from Eqs.(4) and (5), σ_2 depends on only one contact interaction parameter ($\epsilon_{\rm LR}$), σ_P is two-parameter dependent ($\epsilon_{\rm RR}$ and $\epsilon_{\rm LL}$), and σ_1 depends on all three parameters. Therefore, the derivation

of the model-independent constraints on the CI couplings requires the combination all polarized observables of Eq. (7). In this regard, to emphasize the role of polarization, one can observe from Eqs. (3)-(5) that in the unpolarized case $P_1 = P_2 = 0$, where only σ_1 and σ_2 appear, the interference of the $\epsilon_{\rm LR}$ term with the SM amplitude in A_0 and A_- has opposite signs, leading to a partial cancellation for $-t \sim s$. Consequently, as briefly anticipated in Sect. 1, one expects the unpolarized cross section to have reduced sensitivity to $\epsilon_{\rm LR}$. Conversely, $\epsilon_{\rm LR}$ is *directly* accessible from $\mathrm{d}\sigma_2$, *via* polarized cross sections as in Eq. (7). Also, considering that numerically $g_{\rm L}^2 \cong g_{\rm R}^2$, the parameters $\epsilon_{\rm LL}$ and $\epsilon_{\rm RR}$ contribute to the unpolarized cross section through A_+ with equal coefficients, so that, in general, only correlations of the form $|\epsilon_{\rm LL} + \epsilon_{\rm RR}| < \text{const}$, and not finite allowed regions, could be derived in this case.

To make contact to the experiment we take $P_1 = 0.8$ and $P_2 = 0.6$, and impose a cut in the forward and backward directions. Specifically, we consider the cut angular range $|\cos\theta| < 0.9$ and divide it into nine equal-size bins of width $\Delta z = 0.2$ ($z \equiv \cos\theta$). We also introduce the experimental efficiency, ϵ, for detecting the final e^+e^- pair and, according to the LEP2 experience, $\epsilon = 0.9$ is assumed.

We then define the four, directly measurable, event rates integrated over each bin:

$$N_{++}, \quad N_{--}, \quad N_{+-}, \quad N_{-+}, \tag{8}$$

and ($\alpha\beta = ++$, etc.):

$$N_{\alpha\beta}^{\rm bin} = \frac{1}{4}\mathcal{L}_{\rm int}\,\epsilon \int_{\rm bin} (\mathrm{d}\sigma_{\alpha\beta}/\mathrm{d}z)\mathrm{d}z. \tag{9}$$

In Eq. (9), $\mathcal{L}_{\rm int}$ is the time-integrated luminosity, which is assumed to be equally divided among over the four combinations of electron and positron beams polarization defined in Eqs. (6).

In Fig. 1, the bin-integrated angular distributions of $N_{++}^{\rm bin}$ and $N_{+-}^{\rm bin}$ in the SM at $\sqrt{s} =$ 500 GeV and $\mathcal{L}_{\rm int} = 50$ fb^{-1} are presented as histograms. Here, the SM cross sections have been evaluated by means of the effective Born approximation [18, 19]. The typical forward peak, dominated by the t-channel photon pole, dramatically shows up, and determines a really large statistics available in the region of small t. The $\cos\theta$ distributions for the other polarization configurations in (6) are similar and, therefore, we do not represent them here.

The next step is to define the relative deviations of the cross sections σ_1, σ_2 and σ_P from the SM predictions, due to the contact interaction. In general, for such deviations, we use the notation:

$$\Delta_{\mathcal{O}} = \frac{\mathcal{O}(SM + CI) - \mathcal{O}(SM)}{\mathcal{O}(SM)}, \tag{10}$$

To get an illustration of the effect of the contact interactions on the observables (7) under consideration, we show in Fig. 2a and Fig. 2b the angular distributions of the relative deviations of $\mathrm{d}\sigma_1$ and $\mathrm{d}\sigma_2$, taking as examples the values of $\mathcal{L}_{\rm int}$ and Λ_{ij} indicated in the captions. The SM predictions are evaluated in the same, effective Born, approximation as in Fig. 1. The deviations are then compared to the expected statistical uncertainties, represented by the vertical bars. Fig. 2a shows that $\mathrm{d}\sigma_1$ is sensitive to contact interactions

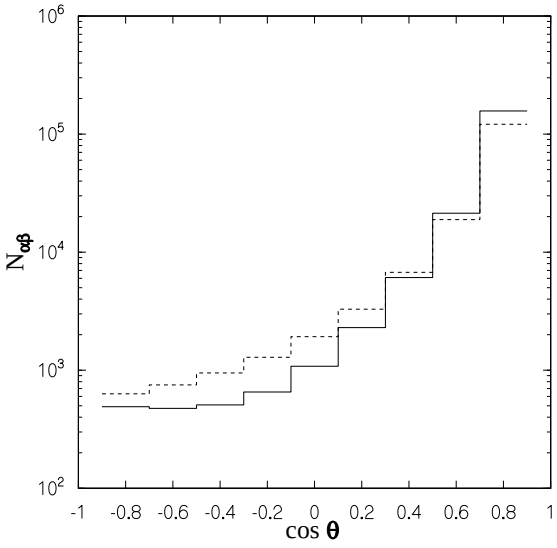

Figure 1: Bin-integrated angular distributions of $N^{\rm bin}_{+-}$ (solid line) and $N^{\rm bin}_{++}$ (dashed line), Eq.(9), in the SM at $\sqrt{s} = 500$ GeV and $\mathcal{L}_{\rm int} = 50$ fb^{-1}.

in the forward region, where the ratio of the 'signal' to the statistical uncertainty increases. Also, it indicates that, for the chosen values of the c.m. energy $\sqrt{s}$ and $\mathcal{L}_{\rm int}$, the reach on Λ_{ij} will be substantially larger than 30 TeV. Conversely, Fig. 2b shows that the sensitivity of $\mathrm{d}\sigma_2$ is almost independent on the chosen kinematical range in $\cos\theta$, leading to a really high sensitivity of this observable to $\epsilon_{\rm LR}$, and to corresponding lower bounds on $\Lambda_{\rm LR}$ potentially larger than 50 TeV. We now proceed to the analysis of the bounds on the contact interaction couplings.

3 Constraints on CI couplings

To assess the sensitivity to the compositeness scale we assume the data to be well described by the SM predictions ($\epsilon_{ij} = 0$), *i.e.,* that no deviation is observed within the foreseen experimental accuracy, and perform a χ^2 analysis of the $\cos\theta$ angular distribution. For each of the observable cross sections, the χ^2 distribution is defined as the sum over the above mentioned nine equal-size $\cos\theta$ bins:

$$\chi^2(\mathcal{O}) = \sum_{\rm bins} \left(\frac{\Delta\mathcal{O}^{\rm bin}}{\delta\mathcal{O}^{\rm bin}} \right)^2 , \tag{11}$$

where $\mathcal{O} = \sigma_1$, σ_2, σ_P and $\sigma^{\rm bin} \equiv \int_{\rm bin}(\mathrm{d}\sigma/\mathrm{d}z)\mathrm{d}z$. In Eq. (11), $\Delta\mathcal{O}$ represents the deviation from the SM prediction, $\Delta\mathcal{O} = \mathcal{O}(SM + CI) - \mathcal{O}(SM)$, that can be easily expressed

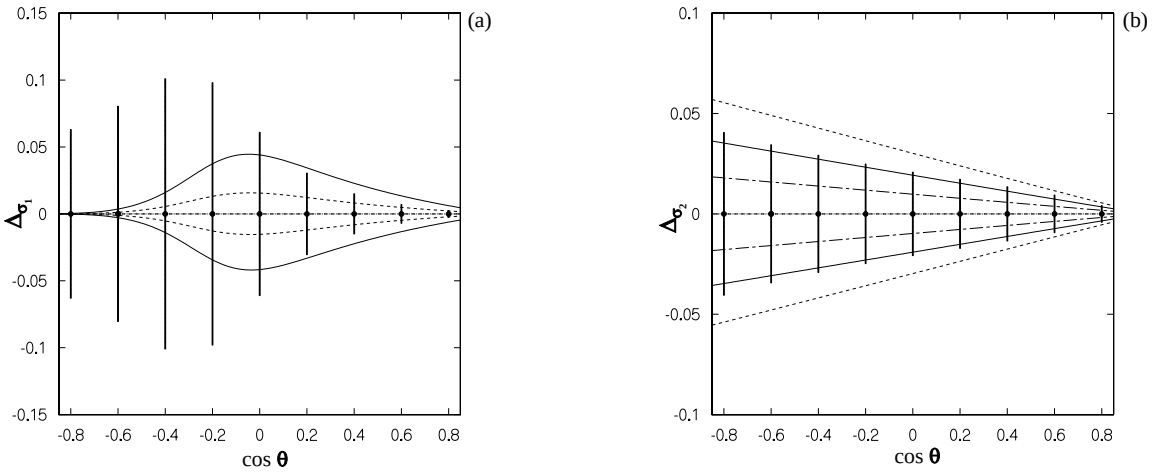

Figure 2: The angular distributions for the relative deviations Δ_{σ_1} (a) at $\Lambda_{\rm RR}$=30 TeV (solid line) and 50 TeV (dashed line), and for Δ_{σ_2} (b) at $\Lambda_{\rm LR}$=40 TeV (dashed line), 50 TeV (solid line), 70 TeV (dot-dashed line). The curves above (below) the horizontal line correspond to negative (positive) interference between contact interaction and SM amplitude. The error bars show the expected statistical error at $\mathcal{L}_{\rm int} = 50$ fb^{-1}.

in terms of the CI couplings by using Eqs. (5), and $\delta\mathcal{O}$ is the expected experimental uncertainty, that combines the statistical and the systematic one.

In the following analysis, the theoretical expectations for the polarized cross sections are evaluated by using the program TOPAZ0 [20, 21], adapted to the present discussion, with $m_{\rm top} = 175$ GeV and $M_H = 120$ GeV. For electron-positron final states, a cut on the acollinearity angle between electron and positron, $\theta_{\rm acol} < 10^\circ$, is applied to select non-radiative events.

Concerning the numerical inputs and assumptions used in the estimate of $\delta\mathcal{O}$, to assess the role of statistics we vary $\mathcal{L}_{\rm int}$ from 50 to 500 fb^{-1} (a quarter of total the running time for each polarization configuration). As for the systematic uncertainty, we take $\delta\mathcal{L}_{\rm int}/\mathcal{L}_{\rm int} = 0.5\%$, $\delta\epsilon/\epsilon = 0.5\%$ and, regarding the electron and positron degrees of polarization, $\delta P_1/P_1 = \delta P_2/P_2 = 0.5$ %.

As a criterion to constrain the allowed values of the contact interaction parameters by the non-observation of the corresponding deviations, we impose $\chi^2 < \chi^2_{\rm CL}$, where the actual value of $\chi^2_{\rm CL}$ specifies the desired 'confidence' level. We take the values $\chi^2_{\rm CL}$ =3.84 and 5.99 for 95% C.L. for a one- and a two-parameter fit, respectively.

We begin the presentation of the numerical results from the consideration of $\epsilon_{\rm LR}$. For this case, the relevant cross section σ_2 depends on $\epsilon_{\rm LR}$ only, see Eqs. (4) and (5) and, therefore, the constraints on that parameter are determined from a one-parameter fit. The model-independent, discovery reach expected at the LC for the corresponding mass scale $\Lambda_{\rm LR}$ is represented, as a function of the integrated luminosity $\mathcal{L}_{\rm int}$, by the solid line in Fig. 3. As expected, the highest luminosity determines the strongest constraints on the

CI couplings.[1] Fig. 3 dramatically shows the really high sensitivity of σ_2, such that the discovery limits on $\Lambda_{\rm LR}$ are the highest, compared to the $\Lambda_{\rm RR}$ and $\Lambda_{\rm LL}$ cases, and can be as large as 110 up to 170 times the total c.m. energy.

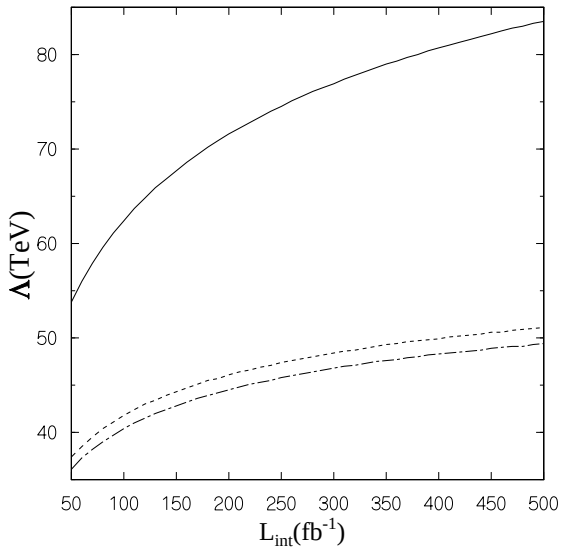

Figure 3: Reach in Λ_{ij} at 95% C.L. *vs.* integrated luminosity $\mathcal{L}_{\rm int}$ obtained from the model-independent analysis for $e^+ + e^- \to e^+ + e^-$ at $E_{\rm c.m.} = 0.5$ TeV, $|P^-| = 0.8$ and $|P^+| = 0.6$, $\Lambda_{\rm LR}$ (solid line), $\Lambda_{\rm LL}$ (dashed line), $\Lambda_{\rm RR}$ (dot-dash line).

Since σ_P simultaneously depends on the two independent CI couplings $\epsilon_{\rm RR}$ and $\epsilon_{\rm LL}$, a two-parameter analysis is needed in this case. Since the terms quadratic in $\epsilon_{\rm LL}$ and $\epsilon_{\rm RR}$ largely cancel leaving the remaining interference to dominate the relevant deviations from the SM, the resulting constraint has the form of a straight band, as depicted in Fig. 4a. Indeed, such a band represents a correlation between the two parameters, rather than a bound around the SM value $\epsilon_{\rm LL} = \epsilon_{\rm RR} = 0$.

In order to get a restricted allowed region around zero, one can combine the band with the exclusion region obtained from σ_1. However, since the latter depends on *all three* contact interaction parameters, see Eqs. (4) and (5), to set constraints in the $(\epsilon_{\rm RR}, \epsilon_{\rm LL})$ plane requires the combination of the σ_1-bounds with the limits on $\epsilon_{\rm LR}$ derived above from σ_2. The bound in the $(\epsilon_{\rm RR}, \epsilon_{\rm LL})$ resulting from this procedure is shown in Fig. 4a and, finally, the shaded ellipse determined by the combination with the band determined by σ_P represents the restricted allowed region around the SM point $\epsilon_{ij} = 0$. With reference to Eq. (11), for the χ^2 analysis this amounts to the consideration of the combined $\chi^2(\sigma_1) + \chi^2(\sigma_P)$. Fig. 4b is essentially a magnification of the shaded region of Fig. 4a, and represents

[1]Such increase with luminosity is somewhat slower than expected from the scaling law $\Lambda \sim (s\mathcal{L}_{\rm int})^{1/4}$, as the effect of the systematic uncertainties competing with the statistical ones.

the model-independent limits on $\epsilon_{\rm LL}$ and $\epsilon_{\rm RR}$ attainable at the considered LC, for two possible values of the integrated luminosity. These bounds are translated into the model-independent reach on the mass scale parameters $\Lambda_{\rm LL}$ and $\Lambda_{\rm RR}$, represented as a function of luminosity in Fig. 3. The fact that such bounds are substantially lower than those for $\Lambda_{\rm LR}$ reflects that a combined two-parameter χ^2 analysis must be used. In this regard, the calculation presented here indicates that not only polarization, but also combinations of measurements of polarized observables are necessary to obtain model-independent bounds on the CI couplings.

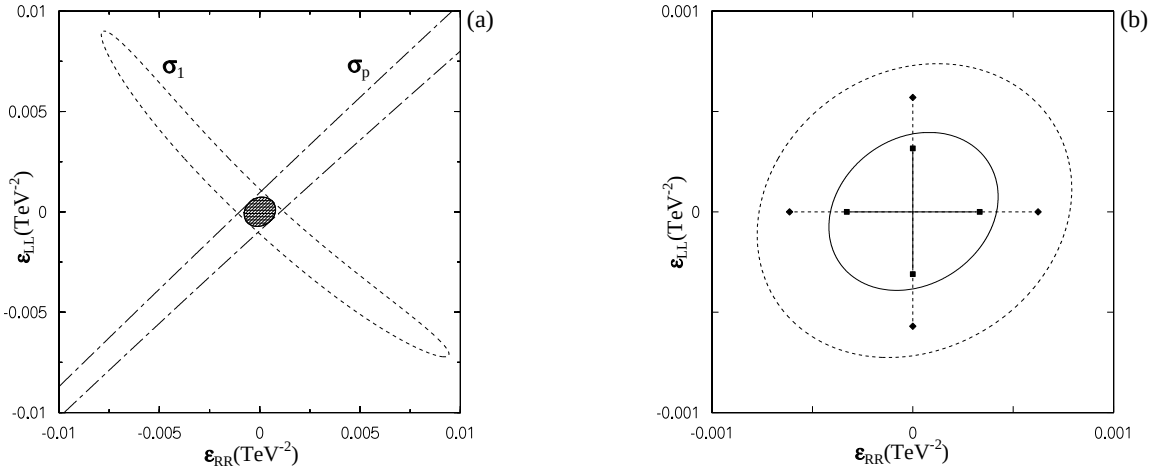

Figure 4: (a) Allowed areas at 95% C.L. on electron contact interaction parameters in the planes $(\epsilon_{\rm RR}, \epsilon_{\rm LL})$, obtained from σ_1 and σ_P at $\sqrt{s} = 500$ GeV and $\mathcal{L}_{\rm int} = 50$ fb^{-1}(a); (b) Combined allowed regions at 95% C.L. obtained from σ_1 and σ_P at $\sqrt{s} = 500$ GeV, $\mathcal{L}_{\rm int} = 50$ fb^{-1} (outer ellipse) and 500 fb^{-1} (inner ellipse).

The crosses in Fig. 4b represent the model-dependent constraints obtainable by taking only one non-zero parameter at a time, instead of two simultaneously non-zero, and independent, as in the analysis discussed above. Similar to the inner and outer ellipses, the shorter and longer arms of the crosses refer to integrated luminosity $\mathcal{L}_{\rm int} = 50$ fb^{-1} and 500 fb^{-1}, respectively. One can note from Fig. 4b that the 'single-parameter' constraints on the individual CI parameters $\epsilon_{\rm RR}$ and $\epsilon_{\rm LL}$ are numerically more stringent, as compared to the model-independent ones. Essentially, this is a reflection of the smaller value of the critical χ^2, $\chi^2_{\rm crit} = 3.84$ corresponding to 95% C.L. with a *one-parameter* fit, and also of a reduced role of correlations among the different observables.

4 Concluding remarks

In the previous sections we have derived limits on the contact interactions relevant to Bhabha scattering by a model-independent analysis that allows to simultaneously account

for all independent couplings as non-vanishing free parameters. The results for the lower bounds on the corresponding mass scales Λ range, depending on the luminosity, from essentially 38 to 50 TeV for the LL and RR cases, and from 54 to 84 TeV for the LR case. The comparison with the numerical results relevant to the $e^+e^- \to \mu^+\mu^-$ channel, derived from a similar analysis [17], is shown in Table 1.

Table 1: Reach in Λ_{ij} at 95% C.L., from the model-independent analysis performed for $e^+e^- \to \mu^+\mu^-$ and e^+e^-, at $E_{\rm c.m.} = 0.5$ TeV, $\mathcal{L}_{\rm int} = 50\,{\rm fb}^{-1}$ and $500\,{\rm fb}^{-1}$, $|P^-| = 0.8$ and $|P^+| = 0.6$.

process	$\mathcal{L}_{\rm int}$ fb^{-1}	$\Lambda_{\rm LL}$ TeV	$\Lambda_{\rm RR}$ TeV	$\Lambda_{\rm LR}$ TeV	$\Lambda_{\rm RL}$ TeV
$e^+e^- \to \mu^+\mu^-$	50	35	35	31	31
	500	47	49	51	52
$e^+e^- \to e^+e^-$	50	38	36	54	
	500	51	49	84	

The table shows that for $\Lambda_{\rm LL}$ and $\Lambda_{\rm RR}$ the restrictions from $e^+e^- \to \mu^+\mu^-$ and $e^+e^- \to e^+e^-$ are qualitatively comparable. Instead, the sensitivity to $\Lambda_{\rm LR}$, and the corresponding lower bound, is dramatically higher in the case of Bhabha scattering. In this regard, this is the consequence of the initial beams longitudinal polarization that allows, by measuring suitable combinations of polarized cross sections, to directly disentangle the coupling $\epsilon_{\rm LR}$. Indeed, without polarization, as previously observed, in general only correlations among couplings, rather that finite allowed regions, could be derived. Alternatively, in the unpolarized case, a one-parameter analysis testing individual models can be performed.

Acknowledgements

I would like to thank Prof. N. Paver for the enjoyable collaboration on the subject matter covered here.

References

[1] E. Eichten, K. Lane and M. E. Peskin, Phys. Rev. Lett. **50** (1983) 811;
R. Rückl, Phys. Lett. B **129** (1983) 363;
E. Eichten, I. Hinchliffe, K. Lane and C. Quigg, Rev. Mod. Phys. **56** (1984) 579;
and references there.

[2] See, *e.g.*: J. A. Aguilar-Saavedra *et al.*, DESY-2001-011, hep-ph/0106315.

[3] D. Abbaneo *et al.* [ALEPH Collaboration], CERN-EP-2000-016.

[4] D. Bourilkov, hep-ph/0104165.

[5] V. Barger, K. Cheung, K. Hagiwara and D. Zeppenfeld, Phys. Rev. D **57** (1998) 391 [hep-ph/9707412];
D. Zeppenfeld and K. Cheung, hep-ph/9810277;
K. Cheung, hep-ph/0106251.

[6] G. Altarelli, J. Ellis, G. F. Giudice, S. Lola and M. L. Mangano, Nucl. Phys. B **506** (1997) 3 [hep-ph/9703276];
R. Casalbuoni, S. De Curtis, D. Dominici and R. Gatto, Phys. Lett. B **460** (1999) 135 [hep-ph/9905568].

[7] A. F. Zarnecki, Eur. Phys. J. C **11** (1999) 539 [hep-ph/9904334].

[8] A. F. Zarnecki, Nucl. Phys. Proc. Suppl. **79** (1999) 158 [hep-ph/9905565].

[9] V. Barger and K. Cheung, Phys. Lett. B **480** (2000) 149 [hep-ph/0002259].

[10] B. Schrempp, F. Schrempp, N. Wermes and D. Zeppenfeld, Nucl. Phys. B **296** (1988) 1.

[11] D. Bardin, W. Hollik and T. Riemann, Z. Phys. C **49** (1991) 485.

[12] T. L. Barklow, Int. J. Mod. Phys. A **11** (1996) 1579.

[13] E. J. Eichten and S. Keller, in *Batavia 1997: Physics at the first muon collider*, FERMILAB-CONF-98-011-T (1998) [hep-ph/9801258].

[14] M. Beccaria, F. M. Renard, S. Spagnolo and C. Verzegnassi, Phys. Rev. D **62** (2000) 053003 [hep-ph/000210].

[15] S. Riemann, LC Note LC-TH-2001-007 (2001).

[16] A. A. Babich, P. Osland, A. A. Pankov and N. Paver, Phys. Lett. B **476** (2000) 95 [hep-ph/9910403]; Phys. Lett. B **481** (2000) 263 [hep-ph/0003253]; LC Note LC-TH-2001-021 (2001) [hep-ph/0101150].

[17] A. A. Babich, P. Osland, A. A. Pankov and N. Paver, hep-ph/0107159, to appear in Phys. Lett. B.

[18] M. Consoli, W. Hollik and F. Jegerlehner, CERN-TH-5527-89 *Presented at Workshop on Z Physics at LEP.*

[19] G. Altarelli, R. Casalbuoni, D. Dominici, F. Feruglio and R. Gatto, Nucl. Phys. B **342** (1990) 15.

[20] G. Montagna, F. Piccinini, O. Nicrosini, G. Passarino and R. Pittau, Nucl. Phys. B **401** (1993) 3.

[21] G. Montagna, O. Nicrosini, F. Piccinini and G. Passarino, Comput. Phys. Commun. **76** (1993) 328; Comput. Phys. Commun. **117** (1999) 278 [hep-ph/9804211].